A Hybrid Coupled General Circulation Model for El Niño Studies

J. DAVID NEELIN

Department of Atmospheric Sciences, U.C.L.A., Los Angeles, California

(Manuscript received 10 August 1989, in final form 2 November 1989)

ABSTRACT

A model is developed for tropical air–sea interaction studies, which is intermediate in complexity between the large coupled general circulation models (coupled GCMs) coming into use and the simple two-level models with which pioneering El Niño–Southern Oscillation studies were carried out. The model consists of a stripped-down tropical Pacific ocean GCM, coupled to an atmospheric model which is sufficiently simple that steady state solutions may be found for low level flow and surface stress, given oceanic boundary conditions. This hybrid coupling of an ocean GCM to a steady atmospheric model permits examination of the nature of interannual coupled oscillations in the absence of atmospheric noise. Tests of the atmospheric model against an atmospheric GCM simulation of El Niño anomalies are presented, and the ocean model climatology is examined under several different conditions. Experiments with the coupled model exhibit a variety of behaviors within a realistic parameter range. These indicate a partial bifurcation diagram in which the coupled system undergoes a Hopf bifurcation from a stable climatology, giving rise to sustained El Niño-period oscillations. The amplitude, period and eastward extent of these oscillations increase with the strength of coupling and the El Niño-period oscillation itself becomes unstable to a higher frequency coupled mode which coexists with it and may affect predictability. The difference between these flow regimes may be relevant to results found by other investigators in coupled GCM experiments.

1. Introduction

The importance of interannual climate variability associated with El Niño and the Southern Oscillation (ENSO) has led to considerable recent interest in tropical ocean–atmosphere coupled modeling. Early studies have been carried out with coupled shallow water or two-level models, notably Philander et al. (1984), Hirst (1986), Zebiak and Cane (1987), Schopf and Suarez (1988) and Battisti (1988). The first two of these are among the studies with linear models pointing to the possibility of instability of the mean state of the tropical ocean–atmosphere system by a variety of feedback mechanisms. The last three are nonlinear models which simulate equilibrated cycles of a several-year period resembling El Niño.

Currently a few groups are undertaking to create coupled models for ENSO studies in which both oceanic and atmospheric components consist of large general circulation models. These models will be referred to as coupled GCMs or CGCMs. Such efforts are underway at the Geophysical Fluid Dynamics Laboratory (GFDL) in Princeton, at the Max Planck Institute für Meteorologie (MPIM) in Hamburg, and at the British Meteorological Office, among others. The approach to coupled GCMs taken by the group of Philander et al. at GFDL is straightforward: an atmospheric GCM which is in current use for atmospheric climate studies (the GFDL climate group model; Manabe et al. 1974) and a Pacific ocean GCM, which has been previously developed and tested in simulations with specified atmospheric boundary conditions (Philander and Pacanowski 1984), are directly coupled by linking the wind stress and heat flux boundary conditions of the two models. The Hamburg group uses a more complicated interfacial condition because of climate drift problems. The enormous computer resources required by these coupled GCMs make it difficult to carry out more than a single simulation of the duration (order of two decades) required to examine the interannual variability of the models.

Because the CGCMs are costly to run and because their complexity makes it difficult to diagnose the modeled phenomena, simpler models such as those mentioned above will remain valuable tools for the eventual understanding of tropical air–sea interactions. The model described here lies at a level of complexity intermediate between these two classes, since it incorporates an ocean GCM but uses an atmospheric model which is much simpler than an atmospheric GCM. Because of this hybrid coupling of an ocean GCM to a steady atmospheric model, the terminology "hybrid coupled model" or "hybrid coupled GCM" (HGCM for brevity) will be used. This model is designed to occupy a particular niche in the hierarchy of coupled models, which makes it suitable for addressing ques-

Corresponding author address: Dr. J. David Neelin, Department of Atmospheric Sciences, University of California, 405 Hilgard Avenue, Los Angeles, CA 90024.

tions concerning the fundamental nature of the coupled variability which may be found in coupled GCMs and in ENSO.

The choice of coupling an ocean GCM to a simpler atmospheric model was made in order to eliminate atmospheric "noise" from the coupled system. Atmospheric GCMs produce a wide spectrum of variability which is independent of coupled processes. The inherent high frequency variability can considerably disrupt coupled oscillations on interannual time scales. This makes it difficult to determine whether they are inherently chaotic, or regular oscillations disrupted by noise, or even a series of events each of which is set off by an atmospheric perturbation. The underlying hypothesis of this model, consistent with the results of the simpler coupled models, is that atmospheric noise is not essential to the oscillations. Ideally, to the extent that the simple atmospheric model can mimic the time-average response of the atmospheric GCM, the hybrid coupled model would represent a distillation of the underlying oscillation mechanism in the CGCMs as it would appear in absence of atmospheric noise. While the effect of atmospheric variability on the coupled system may be considerable in the CGCMs, it is nonetheless worthwhile to understand the dynamics of a similar system in which temporal variability depends entirely on the coupling.

The purpose of this paper is to describe the model and give an indication of the complexity of its behavior. More detailed analysis of the form and mechanism of its interannual variability will be described in further work. The ocean model, its climatology, and its response to wind bursts are described in sections 2, 3 and 4, respectively. The atmospheric model response for ENSO anomalies is investigated in section 5 and the coupling of atmospheric and oceanic models is outlined in section 6. Initial experiments with the coupled model are described in section 7 and discussed in section 8.

2. The ocean model

The ocean GCM of Bryan and Cox (1968) has been adapted by Philander and Pacanowski (1981a) to include Richardson number-dependent vertical mixing for tropical ocean modeling. The finite differencing schemes are discussed in Bryan (1969). When forced with observed wind stress, the model has been shown to realistically reproduce the seasonal cycle in the Atlantic (Philander and Pacanowski 1984), the 1982–83 El Niño (Philander and Siegel 1985), and the seasonal cycle in the tropical Pacific (Philander et al. 1987, hereafter referred to as PHS). The principal effect of the Richardson number-dependent mixing is to produce a sharper, more realistic thermocline. When a constant coefficient of vertical mixing is used (Philander and Pacanowski 1980), the strong vertical temperature gradient found in observations becomes diffuse within a few hundred days and the strength of the undercurrent is sensitive to the value of this coefficient.

The response of this tropical ocean GCM to a variety of idealized wind forcings has also been investigated (Philander 1981; Philander and Pacanowski 1981a; Philander and Pacanowski 1981b). In these experiments, a linearized equation of state is used, with a density of 1 g cm^{-3} at $T = 0$°C and a thermal expansion coefficient of 0.0002 g (cm^3 °C)$^{-1}$. Effects of salinity are ignored. The linear equation of state is also adopted here, since it seems adequate to capture much of the important dynamics of the tropical oceans.

The resolution of the ocean GCM is reduced by roughly a factor of three in every direction relative to the PHS version. This permits extended integrations while still giving a reasonable simulation. A spacing of 1° latitude is used in the equatorial band between 10°S and 10°N, with the mesh spacing increasing smoothly to 4° at the southern boundary at 30°S and 5.6° at the northern boundary at 50°N. The latitudinal domain is chosen for consistency with PHS and so as not to cut the subtropical gyre in the northern Pacific with an artificial wall. A longitudinal mesh spacing of 3° is used. Realistic coasts are not included, but the domain of the box is very similar to the Pacific Ocean, reaching from 130°E to 80°W. The bottom is flat at a depth of 4150 m. Ten levels are used in the vertical; the top three layers are each 20 m thick and seven levels occur above 300 meters in the thermocline region. A timestep of 3 hours is used, the maximum timestep being limited by the stability of the explicit vertical mixing scheme. A nine-level version was also tested, but judged to give unsatisfactory simulation of sea surface temperature (SST).

Near the north and south boundaries thermal damping towards observed annual average temperatures from Levitus (1982) is included. The observations are extrapolated through land points where necessary. The damping coefficient decreases exponentially from (5 days)$^{-1}$ at the walls to (2000 day)$^{-1}$ at 15°S and 26°N. The observed temperature field is also used to initialize the integrations. A Laplacian horizontal mixing coefficient of 4×10^7 cm^2 s^{-1} is used, with slightly higher values near the north and south boundaries. A higher value is also used within about 9° of the western boundary to spread the western boundary current for numerical reasons. This has little effect on the climatology except for the meridional current in the west. Its effect on reflection of long waves has not yet been tested; possible effects on coupled oscillations will be discussed later.

The surface stress boundary condition applied to the model for the simulation of the climatology was obtained from observations by Hellerman and Rosenstein (1983). The annual average wind stress was used, but the Hellerman and Rosenstein values were multiplied by a factor of 0.7 since they are considered to be too strong by about this amount (Harrison 1989, finds large

regions in which a new estimate of the wind stress is 25–30% smaller in the trades and 20–30% smaller in the westerlies, with curl magnitudes being 20–50% smaller in the trades; patterns remain similar between the two estimates in all fields). The heat flux across the ocean surface is parameterized exactly as in PHS, with radiative fluxes an idealized function of latitude. Sensible and latent heat fluxes are given by bulk aerodynamic formulae with a constant relative humidity of 0.8 and the atmospheric temperature just above the ocean surface specified from observations (Levitus 1982).

3. Ocean climatology

Three different ocean climatologies were employed in the series of coupled experiments described in section 7. For each of these climatologies, the ocean was spun up from rest to a steady state with constant surface stress and air temperature applied in the upper boundary condition. Equatorial currents and horizontal temperature gradients came into adjustment by the ninth or tenth month, roughly the transit time of a wave front back and forth across the basin. SST was also approximately adjusted by this time, but the time scale for adjustment of the temperature at depth was considerably longer. In two of the cases, referred to as Clim-I and Clim-II, the initial temperature profile specified from observations was not far from the eventual equilibrium, so a reasonable approximation to the steady state was reached within three years. In the third case, Clim-III, the initial temperature profile was specified in an idealized form with a larger total heat content than the observed temperature field. The vertical profile from 170°E in the western Pacific, which has warm surface temperatures and a deep thermocline, was used as the initial profile all along the equator. Off the equator, initial values were specified by linear interpolation in latitude to typical profiles at 20°N and 15°S. This third climatology was spun up for 1.5 years to a state in which the currents and horizontal temperature gradients were steady but in which the heat content was slowly adjusting toward equilibrium on a decadal time scale. For the purposes at hand, this Clim-III may be regarded as effectively a steady state, although on a longer time scale it is not.

Climatology-I is shown in Fig. 1. The SST (Fig. 1a) is the most important field as far as coupling to an atmospheric model is concerned. The ocean model produced a very reasonable climatology, with a warm pool of roughly the right extent in the western equatorial Pacific and cold water along the equator and the coast of "South America." The Indonesian warm water is correctly divided into two lobes; the larger lobe, south of the equator, forces the South Pacific convergence zone when the atmospheric model is included. The warmest water is about 31°C, slightly warmer than observed but well within reason. The position of the 28° isotherm is quite realistic. In the east, the cold water south of the equator is not quite extensive nor cold enough and it does not join with the cold tongue along the equator, perhaps for lack of a realistic coastline.

All in all, it is surprising how realistic an SST field can be obtained despite the box geography. The position of the warm water north of the equator, for instance, is correctly modeled, its position determined primarily by the specified wind stress. The pool of warm water around 10°N, 110°W is also created by the stress field. In the coupled model, it produces a convergence zone similar to that found over Central America in observations. The main deficiency in the simulation, from the point of view of coupled modeling, is that the equatorial cold tongue is slightly too strong and extends too far west relative to observations. At the western edge of the cold tongue, the 27° and 26° isotherms are as far west as during the cold phase of a composite El Niño (Rasmusson and Carpenter 1982). This is a deficiency commonly encountered in GCM simulations of the Pacific ocean. At depth, the structure of the temperature field at depth along the equator is very reasonable, (as shown in Fig. 1b). The deepening of the thermocline towards the west and the vertical gradients in the thermocline are in agreement with the PHS simulation.

One fortunate circumstance, as far as coupled modeling is concerned, is that there are no equatorial long waves present, as may be seen from the SST field. The model converges to a true steady state, rather than a statistical climatology with three week oscillations along the equatorial wave guide in the eastern Pacific. This is convenient for a number of reasons. Besides making the longer scale behavior easier to see, the period over which SST is averaged for input to the atmospheric model becomes much less important. The long waves are generated by instability of the zonal surface currents near the equator when the latitudinal shear is sufficiently strong (Philander 1976, 1978). It happens that the currents in this climatology are stable. This is reasonable for an annual average climatology, since observed long waves disappear in boreal spring.

The structure of the currents with depth in the upper ocean may be seen in the latitude–depth cross-section at 149°W in Fig. 1c. The eastward Equatorial Undercurrent is prominent, with a maximum of 60 cm s^{-1} at a depth of 120 m. The Undercurrent extends across essentially the whole basin at this depth, with the maximum occurring at a shallower depth to the east and slightly deeper to the west. The westward equatorial surface current also reaches a maximum of 60 cm s^{-1}. The eastward Countercurrent, just north of the equator, surfaces only west of the date line. At this longitude, it just breaks the surface. Slightly subsurface, at 50 m, it extends right across the basin with a velocity of 10 cm s^{-1} over a substantial portion. This is reasonable for forcing by annual averaged winds, as it is characteristic of the March–April–May phase of the seasonal cycle in the PHS simulation.

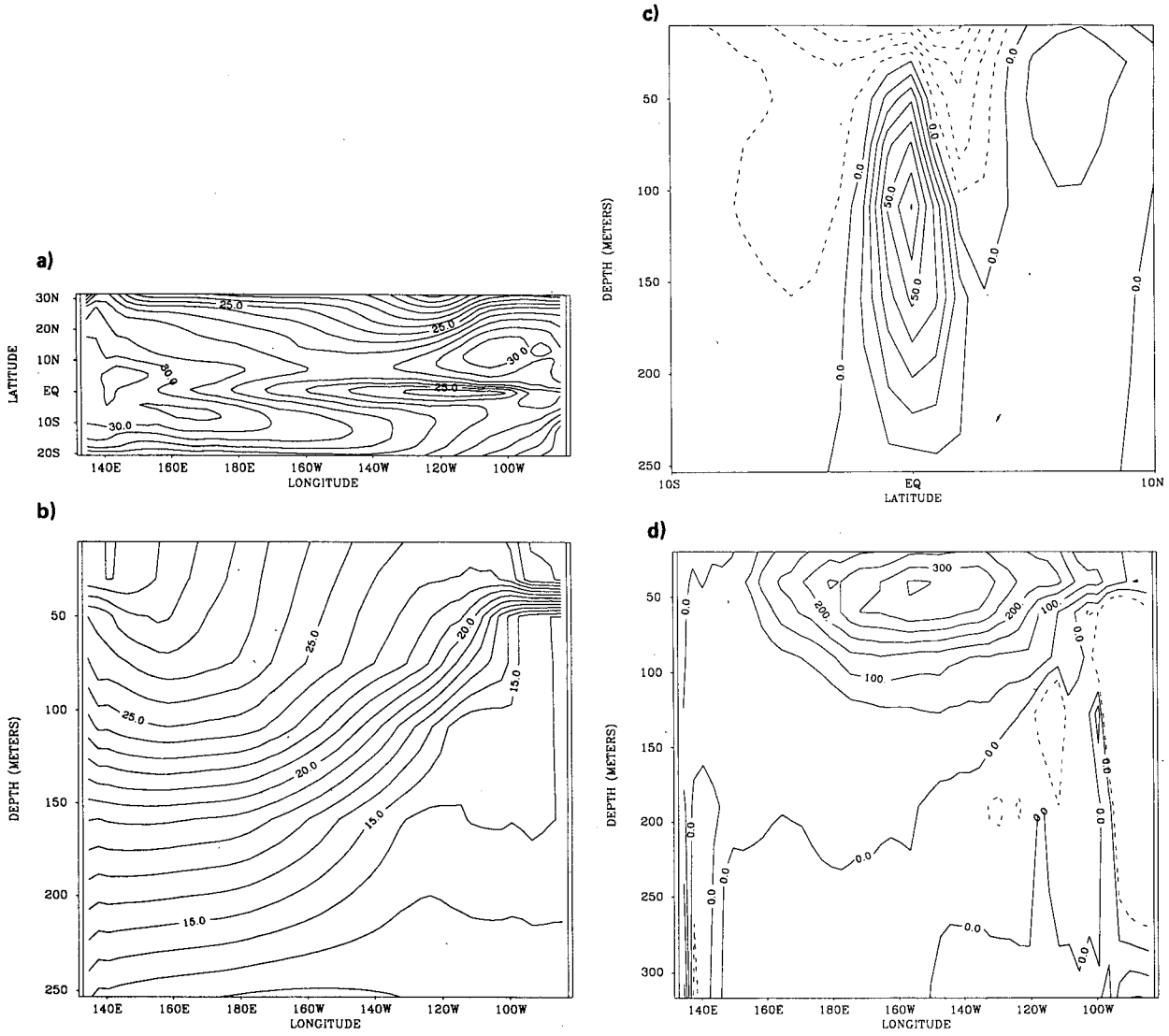

FIG. 1. Ocean Climatology I. Instantaneous fields at the end of the three year spin-up. (a) SST, (b) temperature section along the equator, (c) zonal current at 149°W, (d) vertical velocity along the equator.

The equatorial upwelling may be seen in a longitude–depth section along the equator in Fig. 1d. The strength of the upwelling compares very well with the PHS simulation. The upwelling extends down to 150 to 200 m, with the maximum occurring at 40 to 60 m depth. The upwelling remains strong as far west as 170°E, which may be one reason that the equatorial cold tongue extends so far west. The upwelling is confined to a narrow region within about 2° of the equator, compensated by widespread off-equatorial downwelling. A narrow region of downwelling associated with the curl of the stress occurs just north of the equator as in observations and the PHS simulation.

One slightly unrealistic feature of the box geometry is a northward flowing western boundary current which extends from 10°S to 40°N driven by the wind curl over the basin. In realistic geography, this would be spread out by the gradual decrease in depth toward the west and by continental and island topography. It is believed that this feature will not seriously affect the simulation.

The net heat flux into the ocean surface is positive in most regions, especially in a band along the equator where cold water temperatures tend to reduce evaporation. In the subtropics, there are regions where the ocean loses heat to the atmosphere, largely because of high wind speeds causing increased evaporation. Heat transported poleward to high latitudes is removed by the Newtonian cooling.

Clim-I has too cold and too extensive an equatorial cold tongue relative to observations. During the course of the coupled modeling experiments, it was hypoth-

esized that this tends to work against interannual oscillations. It thus seemed of interest to consider a climatology in which the specified climatological wind stress was weaker. Clim-II is the result of a three year spin up using the same stress field as Clim-I, but with its strength everywhere reduced by a multiplicative factor of 0.6. Otherwise, everything is as for Climatology I. The strength of the specified climatological wind stress thus becomes a simple and understandable parameter whose effects on the coupled system prove interesting to examine. It also serves as an expedient means of reducing the strength of the cold tongue. Other means of varying this aspect of the climatology, such as changing the vertical mixing parameters, would be considerably less straightforward to describe and understand although, in the long run, such exploration may prove desirable if the changes can be put on a more sound physical basis.

The resulting Clim-II SST and equatorial temperature section are shown in Fig. 2. The coldest part of the cold tongue is not quite as cold as observed but the westward extension of it is actually more realistic than in Clim-I. The vertical and longitudinal structure of the thermocline is not strongly affected. The vertical velocity field is reduced almost in proportion to the reduction in wind stress while the currents are not reduced by as much due to the importance of nonlinearity in the momentum balance.

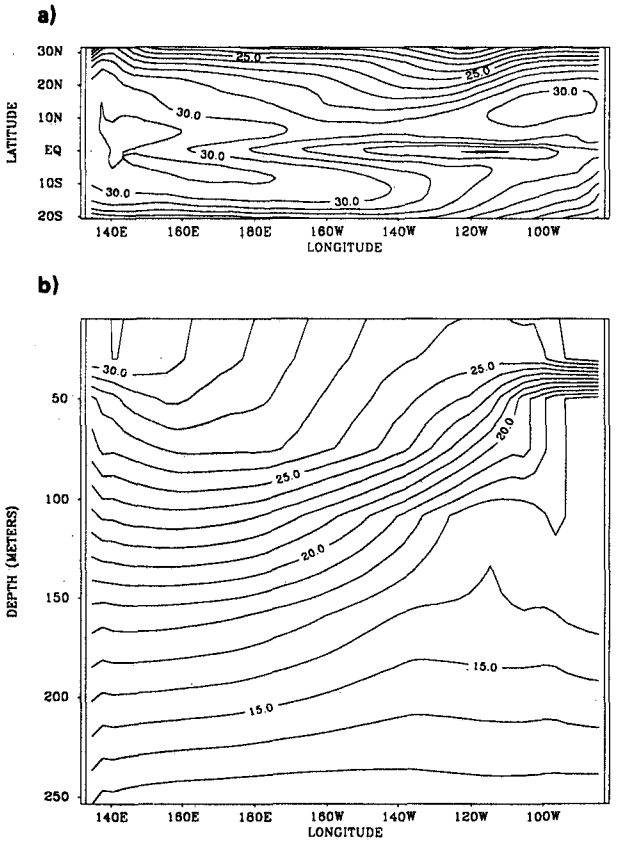

FIG. 2. As for Fig. 1, but for Climatology II. (a) SST and (b) temperature section along the equator.

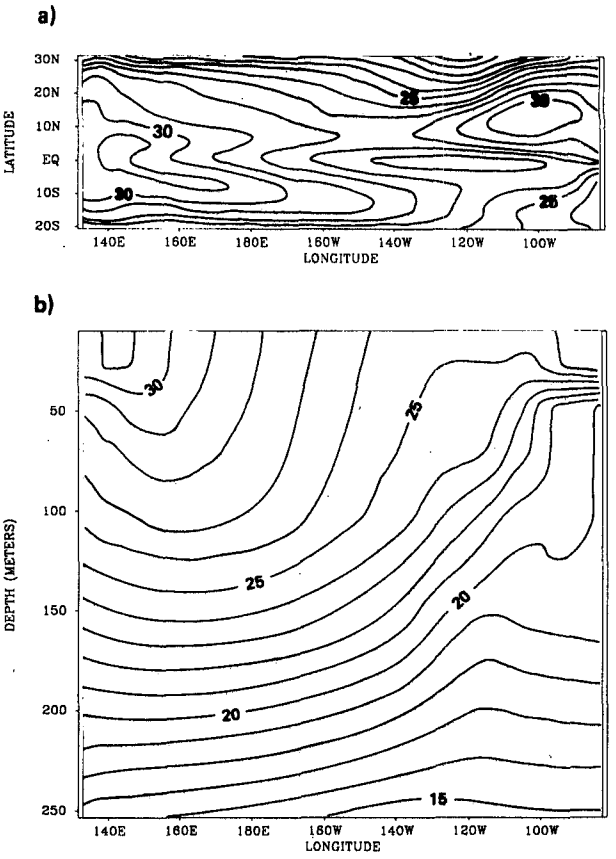

FIG. 3. As for Fig. 2, but for Climatology III at the end of the 1.5 year spinup.

As described above, Clim-III was designed to have a larger equatorial heat content than Clim-I. SST and the equatorial temperature section are seen in Fig. 3. The overall SST pattern differs from Clim-I in that the cold tongue is not as cold. Current and upwelling patterns are rather similar to Clim-I so the reduction of the cold tongue occurs for different dynamical reasons than in Clim-II. The vertical section of temperature reveals the strongest differences; the thermocline is much deeper and less sharp than in the other two runs. Roughly speaking, the 20° isotherm replaces the 15° isotherm, so the upwelled water is considerably warmer.

4. Response of the ocean to a westerly stress anomaly

A westerly stress anomaly in the western Pacific tends to accelerate eastward currents and move warm water towards the east, as occurs in the early stages of El Niño (Rasmusson and Carpenter 1982). The response of the ocean model to such an anomaly serves as a control run for similar experiments conducted with the coupled model, described in section 7. The initial

wind stress anomaly used in these experiments was also designed to be roughly consistent with coupled GCM experiments of Latif et al. (1988).

The integration was begun from Climatology-II, by adding a stress anomaly of 0.3 dyn cm^{-2} between 10°S and 10°N and west of 170°W for the first month of the run. The response of the SST and zonal velocity fields may be seen in Fig. 4. During the time that the stress anomaly is applied, eastward currents are forced in the region of the stress anomaly. Wavefronts may be seen propagating eastward from the boundaries of the patch. Estimating the phase speed from the region of westerly anomalies (weakened easterly current) which reaches the east coast during the second month of the run gives 2.5 m s^{-1}. This is reasonable for the gravest internal Kelvin mode, and in agreement with the phase speed found in Philander and Pacanowski (1980). However, they find that it is the second gravest vertical mode which is most noticeable in bringing the ocean fields to adjustment in a similar switch on experiment. The phase speed of this is 1.45 m s^{-1} in their model. This is about the apparent speed of propagation of information from the west coast after the stress anomaly is switched off, so it is possible that both modes are important in the adjustment. Rossby waves complete the adjustment, traveling back from the east coast with an apparent phase speed of a little over 1 m s^{-1} for the fastest mode. It is also worth noting that in both SST and surface current fields the local response within the region of wind forcing is significantly larger than the remote response associated with wave propagation.

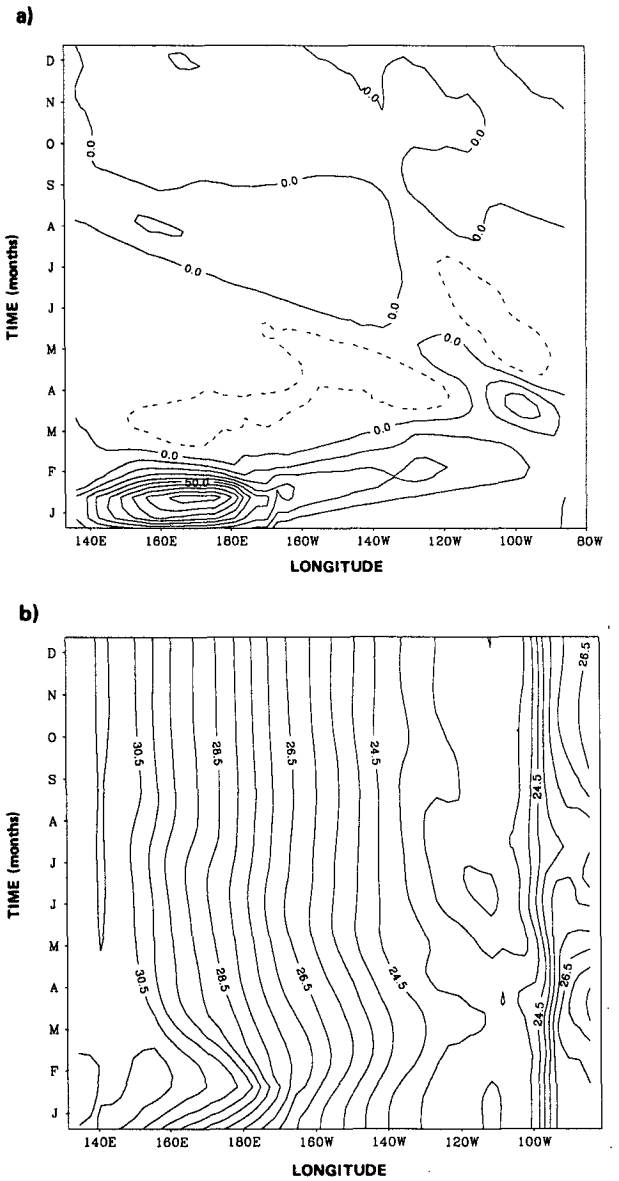

FIG. 4. Time–longitude plots over one year of an ocean experiment with a westerly wind anomaly applied west of 170°E for the first month: (a) zonal surface current anomaly at the equator (contour interval 10 cm s^{-1}), (b) SST at the equator (contour interval 0.5 degrees).

In the SST field, warm water moves eastward along the equator, with the isotherms in the west reaching their maximum displacement just after the stress anomaly is switched off. The SST returns rapidly to equilibrium. It is essentially adjusted by the time the information from the west coast at the switch-off reaches the region of strongest thermocline displacement in the third month. By the fifth month, the perturbation from the stress anomaly has disappeared completely.

5. The atmospheric model

Simple, two-level models of the tropical atmosphere have already seen considerable use in coupled ocean–atmosphere models, despite the fact that the processes involved are not yet well understood and the accuracy of the models has not been rigorously demonstrated. One reason for this popularity is convenience, the other is the qualitative success of the Gill model for simulating low level flow, given the atmospheric latent heating (Matsuno 1966; Gill 1980). The model of Neelin (1988), hereafter referred to as N, is based on a reinterpretation of the Gill model as a model for the atmospheric boundary layer with heavy damping due to vertical diffusion of momentum by boundary layer turbulence.[1] Viewed in this manner, the N version of the Gill model gives surface stress directly when forced

[1] The model of Lindzen and Nigam (1987) uses the same interpretation of the momentum equations, but further includes forcing by horizontal pressure gradients in the boundary layer, associated with the gradients of SST. A brief discussion of the interpretation of the Gill model in terms of the Lindzen and Nigam model may be found in Neelin (1989).

by the vertical velocity at the top of the trade cumulus boundary layer (or by latent heating, since this is closely related to the vertical velocity). The model does very well when compared to the results of an atmospheric GCM (AGCM) experiment, both for the climatology and for ENSO composite anomalies.

The success of the Gill model in this respect amounts to demonstrating that the nondivergent part of the wind field can be obtained from a given divergence using a linearly damped vorticity equation, where the damping time, about 2 days, is the coefficient relating surface stress to boundary layer mass transport. However, this is only part of the task of modeling the tropical atmosphere. A much more difficult problem is to obtain the boundary layer convergence (or vertical velocity, or latent heating) from given boundary conditions. Previous approaches have simply taken the latent heating to be a given function of SST (Philander et al. 1984; Anderson and McCreary 1985) or else assumed that latent heating anomalies are caused by flux anomalies out of the sea surface, intensified in one manner or another by a parameterized atmospheric feedback (Webster 1981; Zebiak 1986; Davey and Gill 1987). Neelin and Held (1987, NH hereafter) argue that surface fluxes are not the only process which can affect the location of the convection and that warm SSTs can directly affect the position of convection through the moist stability. Neelin and Held propose a simple two-layer model for the midtropospheric latent heating and vertical velocity at the top of the boundary layer in the tropics, based on consideration of the moist static energy budget. It should be pointed out that another recent simple steady state model for tropical boundary layer flow, by Lindzen and Nigam (1987), is based on a different physical process and assumptions. The purpose of the present section is simply to show that a combination of the NH and N models gives a useful simulation of the vertical velocity at the top of the boundary layer and surface stress for ENSO anomalies, including a reasonable approximation to the nonlinearity of the response to SST, compared to an AGCM simulation. In future work, the sensitivity of the coupled system to the choice of atmospheric model will be evaluated by running comparable experiments using the Lindzen–Nigam model.

The circulation in the NH model is driven by the net flux of energy, F_{net}, (latent + sensible + net radiative) through the top and bottom of the atmosphere. However, the strong vertical velocities of the tropical convergence zones are more strongly associated with the minima of the gross moist stability, a vertically integrated measure of moist stability of the two-level model. The gross moist stability is much smaller than the dry static stability in the convergence zones since latent heating due to convergence of lower layer moisture almost compensates for the adiabatic cooling due to rising motion. The parameterizations of moisture and dry static stability in the NH model yield a nonlocal dependence of gross moist stability on SST, the result of which is that the tropical convergence zones tend to occur in regions of maximum total SST. The response to SST in this model is quite nonlinear—a warm anomaly in a region of cold climatological SST has much less effect than the same anomaly would have if added to a region of high SST.

In application to air–sea coupling problems, the interfacial condition includes bulk aerodynamic formulae for the dependence of surface energy fluxes on SST and low level wind. SST affects the low-level convergence both through the surface fluxes and by its direct effect on the moist stability. In the discussion in this section, the flux term, F_{net}, is specified exactly from the AGCM simulation in order to show that this term alone would not lead to a good simulation of the low level convergence and to suggest the importance of the direct effect of SST on the moist stability. The parameterization of moisture on SST has been applied only over ocean points in these results, with moisture over land specified from the AGCM. Care was taken that the parameterized values be consistent with those from the AGCM so that no discontinuities occur at land–ocean boundaries.

The AGCM climatology to which the simple model is compared is the same as that used in N to evaluate the stress-from-omega part of the model. It consists of two 15-year integrations in which observed, time-varying SSTs are prescribed in the tropical Pacific Ocean. The interannual variability associated with ENSO is well described in these experiments. ENSO composites based on six events (the 1969, 1972 and 1976 events from each of the two runs) presented by Lau (1985) are in good agreement with observations. This same atmospheric GCM is also being used in the coupled GCM experiments of Philander et al.

Figure 5a shows the composite ENSO vertical velocity anomaly from the AGCM for the DJF(+1) or "mature" phase of the oscillation in the Rasmusson and Carpenter (1982) terminology. The compositing is for six events as in Lau (1985). In Fig. 5b the AGCM anomaly in F_{net} is shown. Most of this anomaly is due to changes in the surface fluxes, particularly evaporation. The pattern is considerably different from the convergence anomaly. If one removes the effects of moisture convergence from the model and includes only the effects of this flux anomaly, the resulting convergence anomaly has exactly this pattern—agreeing poorly with the AGCM convergence—and is very weak in amplitude. Taking a dry static stability of 10^5 J kg^{-1} (units of dry static energy), the maximum vertical velocity anomaly forced by the surface flux anomaly would only be 1.5×10^{-5} mb s^{-1} compared to 3.5×10^{-3} mb s^{-1} in the AGCM. The surface flux anomaly appears to be related to the SST anomaly, shown in Fig. 5c, but this bears little resemblance to the convergence anomaly. In the easternmost part of the basin, where climatological SST is low, the SST anomaly is

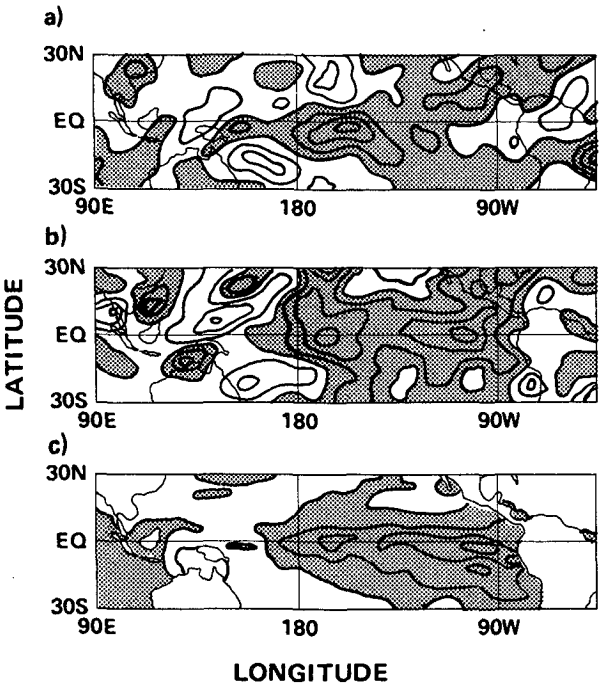

FIG. 5. Atmospheric GCM composite quantities for the DJF(+1) phase of ENSO. (a) Lower tropospheric mass flux convergence anomaly (below 700 mb). Contour interval 1×10^{-3} kg m^{-2} s^{-1} (vertical velocity equivalent 1×10^{-4} mb s^{-1}), stippled where positive. (b) Net flux anomaly (sensible heating + evaporation + net radiative flux). Contour interval 5 W m^{-2}, stippled where positive. (c) SST anomaly used in boundary condition. Contour interval 0.5 degrees, stippled where positive.

ineffective in producing a convergence anomaly. The nonlinearity associated with variations of gross moist stability tends to reproduce this effect in the NH model, since anomalies have more effect in regions of higher climatological SST.

ENSO anomalies are computed by running the simple model separately with total SST and F_{net} fields for the ENSO composite and climatology. The ENSO mature phase convergence anomaly predicted by the simple model over the Pacific is shown in Fig. 6a. The comparison to the AGCM anomaly is quite good. In particular, the location and approximate shape of the central Pacific upward velocity anomaly is reproduced. The model does not properly reproduce divergence regions in the subtropics, but these are not very important features in the ENSO anomalies. It does reproduce the divergence anomalies in the western Pacific to some extent. Certainly, it does far better than would a model based on a local or almost local relationship of heating to the flux anomaly of Fig. 5b or the SST anomaly of Fig. 5c. Such a model would have large, erroneous upward-motion anomalies in the eastern Pacific. In this model the tendency of the flux anomaly to drive convection anomalies in the eastern Pacific is completely overcome by the effect of warm SST in the western and central Pacific, expressed through its effect on the gross moist stability. Because the effective moist static stability is larger in the east, the convective response to F_{net} is reduced in this region. As a result, moisture is exported from this region to neighboring regions with higher moisture and lower moist static stability, where moisture convergence enhances the precipitation. The magnitude of the vertical velocity anomaly is a little large during the DJF(+1) phase since model parameters were chosen for climatological simulation and were not tuned for ENSO anomalies. This occurs to a lesser degree in other phases.

Within the assumptions of the model, the relative effects of the flux term, F_{net}, and of the gross moist stability may be examined by repeating the calculation with the following variations: First, taking F_{net} to remain fixed at its climatological value but using the ENSO DJF(+1) SST to calculate the gross moist stability and, second, taking the gross moist stability to be fixed at its climatological value and using the ENSO values of F_{net}. In each case, the anomaly is calculated as before and is displayed, respectively, in Figs. 6b and 6c.

The convergence anomaly due to the changes in the gross moist stability alone Fig. 6b, is very similar to the results in Fig. 6a. The central Pacific upward ve-

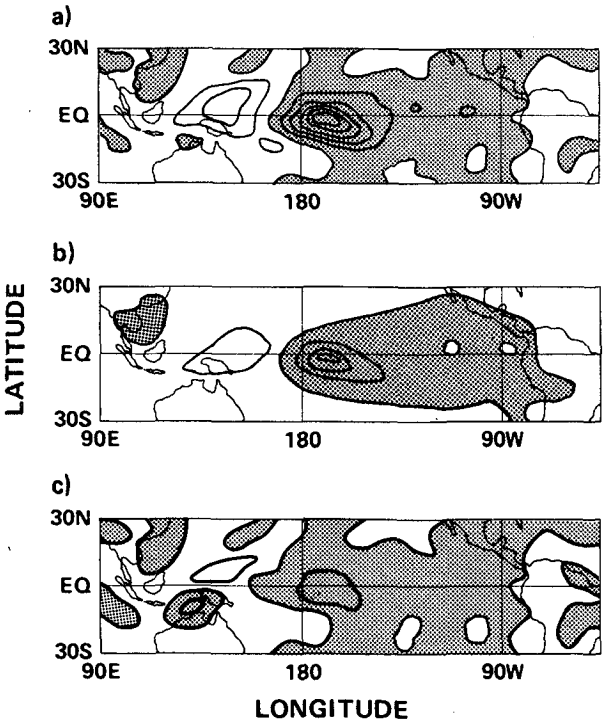

FIG. 6. NH model lower tropospheric mass flux convergence anomaly for the DJF(+1) phase of ENSO. Contour interval 1×10^{-3} kg m^{-2} s^{-1} (vertical velocity equivalent 1×10^{-4} mb s^{-1}), stippled where positive. (a) NH model simulation using ENSO net flux and SST. (b) Using ENSO SST but climatological net flux. (c) Using ENSO net flux but climatological SST.

locity anomaly occurs in about the same location, although it is weaker in magnitude. The anomaly due to the changes in F_{net} alone, in Fig. 6c is also similar, although less strong, showing that the two effects tend to reinforce each other. Because the model is nonlinear, in fact, they reinforce each other by more than a simple addition of Figs. 6b and 6c would give. However, it is important to note that even in the case where the gross moist stability is held fixed, the resulting convergence anomaly is very different in shape and much larger than could be obtained from the flux anomaly alone, without the effects of moisture convergence represented in the gross moist stability. In Fig. 6c the effects of the climatological moist stability are extremely important in shaping the convergence anomaly, as evidenced by the comparison to the flux anomaly in Fig. 5b. Flux anomalies are important only in regions of small climatological moist stability.

Similar results are obtained for other phases of the ENSO cycle. The results of the omega-from-SST model for the total climatology are similar to those found in NH. The general form and movements with season of the tropical convergence zones are well captured. This is almost entirely due to the dependence of the moist stability on SST, since F_{net} is rather slowly varying relative to the sharpness of the convergence zones and has its maxima in the wrong place. The regions of subtropical subsidence, however, are not properly modeled due to the neglect of transient eddy transports which are important in the subtropics. In fact, moist static energy budgets of the AGCM suggest that transient eddy transports may not be truly negligible in the tropics either, but in the context of a simple steady state model, it is impossible to include these effects.

The entire atmospheric model is tested by combining the N and NH models. For the climatology, it was found that the qualitative features were captured but that the poor simulation of subtropical subsidence caused the trade winds to be broadly spread. In the January simulation, the trades straddle the equator, rather than being confined to the Southern Hemisphere. For coupled studies, this wind stress could be expected to force an ocean circulation which would be qualitatively correct in its crudest aspects, but not very satisfactory in terms of detailed simulation of the equatorial ocean climatology.

Much more encouraging results are obtained for the ENSO anomaly simulation. Figure 7 shows the model stress anomalies for JJA(0), DJF(+1) and SON(+1). These may be compared to the AGCM composite stress anomalies shown in N (his Fig. 4). In JJA(0) and DJF(+1), the patch of westerlies in the central Pacific is reproduced in the right location, with roughly the right extent, moving eastward as the event progresses. In DJF(+1), the magnitude is somewhat large because the model omega anomaly is too strong, as noted above. In SON(+1), the easterly anomaly associated with the return to colder temperatures in the east and warmer ones in the west is correctly modeled, although the spatial extent is somewhat too large compared to the AGCM.

The model thus seems to account in a reasonable fashion for the empirical nonlinear relation between SST and vertical velocity anomalies. Although the model could be used for the total wind stress, it is best used as a nonlinear anomaly model (or "flux corrected" model) to predict departures of the stress from climatology as a function of SST. The El Niño anomalies seem to be sufficiently well simulated compared to the AGCM that the model provides a useful simple tropical atmospheric model for ENSO studies. In instances, where the AGCM simulation departs from observations, the simple model does share these deficiencies. For instance, the AGCM simulation of the mature phase winds (Lau 1985) underestimates the meridional component relative to the observational composites of Rasmusson and Carpenter (1982) and the simple model exacerbates this tendency. On the other hand, the simple model does capture an important aspect of both the observed and AGCM composites, namely, that the easterly component of the response to the warm anomaly is much smaller than the westerly component.

6. The coupled model

An additional advantage of setting up the coupled model with the atmospheric component used in flux-corrected mode is that by taking care to define the atmospheric climatology in a manner which is internally consistent to the model, a known, stationary point of the coupled system is constructed. Since only the atmospheric model climatology is replaced by observations, the method used here will be referred to as "one-way flux correction." The atmospheric climatology is defined as the atmospheric model response to the ocean climatology. Since the ocean climatology is in equilibrium with the specified observed wind stress and air temperature, this state will also be a stationary solution of the coupled system. Constructing the system such that one stationary solution is known presents certain practical advantages for understanding the properties of the phase space. Beginning an integration with a perturbation from the stationary point, if the system evolves to a steady state other than the known one, it is clear that there exist multiple equilibria; if the system oscillates, it may be possible to understand its behavior in terms of the instability of the known steady state, and so on.

This approach differs somewhat from the anomaly modeling approach of Zebiak and Cane (1987), and from the flux correction method of Latif et al. (1988), in that the atmospheric climatology is defined via the total response of the atmospheric model to the ocean *model* climatology. The differences from the flux correction of Latif et al. which will be referred to as two-way flux correction, may be summarized as follows.

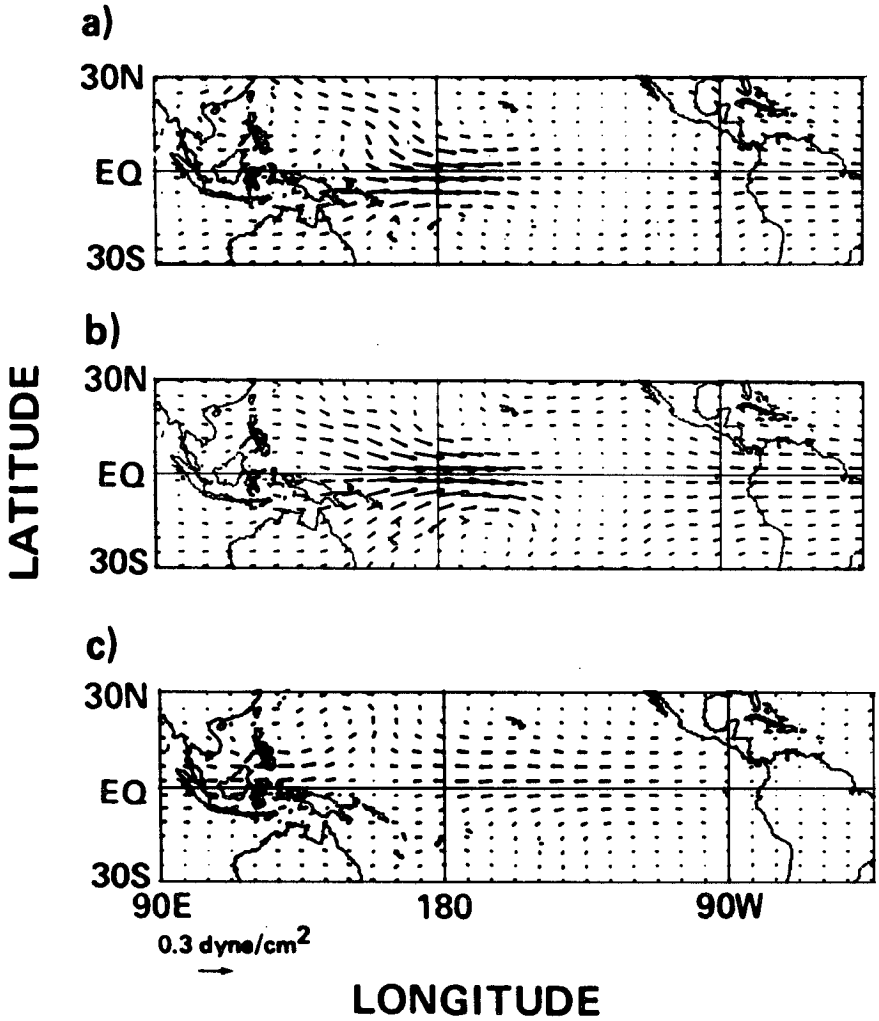

FIG. 7. Simple atmospheric model stress anomalies from ENSO composite SST and net flux. (a) JJA(0); (b) DJF(+1); (c) SON(+1).

In the current coupled model, with one-way flux correction, the ocean component feels a total wind stress which may be written symbolically as

$$\tau = \mathcal{A}(T) - \mathcal{A}(T_0) + \tau_{\text{obs}}$$

where τ_{obs} is the observed climatological wind stress, $\mathcal{A}(T)$ represents the atmospheric model wind stress response as a nonlocal functional of SST, T is the SST of the ocean component of the coupled model and T_0 is the SST of the ocean model climatology defined as the ocean model response to τ_{obs}. The approach corresponding to two-way flux correction in this context, using the same definitions, would have the ocean feel a wind stress

$$\tau = \mathcal{A}(T - T_0 + T_{\text{obs}}) - \mathcal{A}(T_{\text{obs}}) + \tau_{\text{obs}}$$

where T_{obs} is the observed SST. In either case, $T = T_0$ is a stationary point of the coupled system and if the atmospheric model were linear the two approaches would be equivalent. The current approach is preferred because, first, the one-way flux correction replaces only the climatology of the less dependable of the two models by observations and, second, it is hypothesized that nonlinearity will tend to enter in a more consistent way for the particular problem of concern. The atmospheric model responds more strongly in regions to high total SST. If the boundary of the equatorial cold tongue is shifted relative to observations, the current atmospheric model is able to respond appropriately, whereas in the two-way flux correction case an anomaly occuring in the cold tongue region may produce an atmospheric response of magnitude characteristic of warm SST regions, and vice versa. Similar effects occur when linearizing a nonlinear model about the stationary point since the contribution of the atmospheric component to the Jacobian matrix of partial derivatives

of the phase space flow is different under the two schemes. Which of the schemes is preferable will depend on the particular problem of interest.

In the ocean model, the surface flux boundary condition made use of an air temperature which was specified from observations, for consistency with PHS. This is permissible for the climatology (although the ability of the physics to reproduce SST is not as strongly tested as it would be with an interactive boundary layer temperature) since the climatology of air temperature may be regarded as part of the one-way flux correction in the atmospheric component of the coupled model. However, this leaves open the question of how best to model the air temperature anomalies which are certainly influenced by SST anomalies during coupled oscillations. Extrapolating the midtropospheric temperature of the atmospheric model to the surface is a poor solution to this problem since, first, the atmospheric boundary layer air temperature depends little on the temperature in the free atmosphere and, second, two-level models give a poor representation of midtropospheric temperature (it is pointed out in N that this is unimportant to the simulation of surface stress). One reasonable approximation is to assume that the boundary layer air temperature anomalies are simply equal to the SST anomalies. This approximation is made use of in both the Lindzen and Nigam and NH atmospheric models to calculate horizontal pressure gradients and moist static stability, respectively. For the heat flux boundary condition, however, it may tend to underestimate sensible and latent heat fluxes, since the difference between SST and air temperature is the important quantity, not the individual values. The opposite extreme would be to assume that air temperature anomalies cannot respond to SST anomalies at all. This would tend to overestimate latent and sensible heat flux anomalies and thus to damp SST anomalies more strongly than would otherwise be the case. The true behavior of air temperature anomalies will fall between these two extremes; each of these two approximations will be used in turn in order to bracket the behavior which may be expected of the real system. The results presented in this paper make use of the latter approximation. Over- or underestimation of flux anomalies will not strongly affect the response of the atmospheric model, since the contribution of flux anomalies to convergence is of secondary importance. This effect could, however, be significant in other atmospheric models.

In order to provide an indication of the effects of the air temperature on SST, a sensitivity study was performed. A climatological run (Clim-I) was repeated using a different air temperature field: specifically, the climatological air temperature was replaced by its zonal average across the basin at each latitude. Under these boundary conditions, zonal asymmetries in the SST field can only be due to the dynamics, and not to the specified air temperature. Figure 8 shows the resulting SST pattern at the end of 1 year. It is very similar in most respects to the climatology in Fig. 1a. The cold tongue along the equator and the cold region near the South American coast are not quite as cold, and the warm pool in the west is not quite as warm, especially south of the equator. As far as the simulation of the climatology is concerned, it suggests that specifying the air temperature in the surface heat flux boundary condition does tend to constrain the simulation toward observations outside of the dynamically active regions, but that dynamics is more important in the equatorial upwelling region. Nonetheless, for such an enormous change in the air temperature pattern, these changes can be considered relatively minor. For smaller changes in air temperature, such as those associated with ENSO anomalies, the effects would be correspondingly smaller, especially since these occur in the upwelling regions which are dominated by dynamical effects.

Two other quantities were exogenously specified for the atmospheric model. One was the surface temperature outside of the ocean domain. The most straightforward means of doing this was to set the surface temperature for all points outside the basin equal to the zonal average over the basin of the climatological SST. This ensured that the land surface temperatures were consistent with ocean model SST. These temperatures were kept fixed during the course of the coupled run. The same moisture parameterization could then be

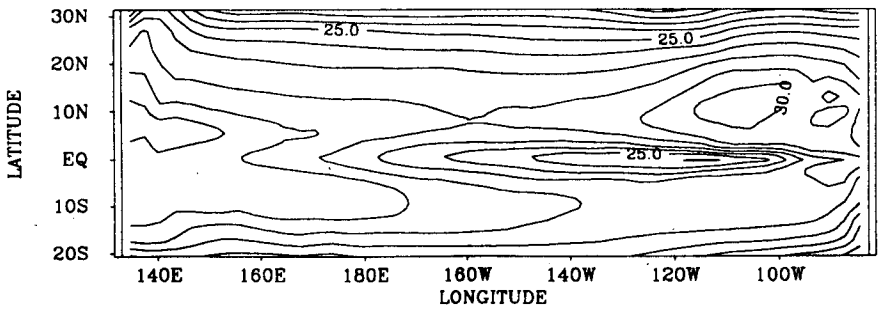

FIG. 8. SST from the ocean climatology experiment with the observed air temperature replaced by its zonal average across the basin at each latitude (otherwise as for Climatology I, Fig. 1a).

applied over both "land" and ocean points in the atmospheric model.

The other quantity specified was the net radiative flux at the top of the atmosphere. The midtropospheric vertical velocity responds to the net flux of energy into the atmospheric column. The net flux at the ocean surface is known from the ocean model and the net flux at the surface over land is zero, taking the heat capacity of land to be zero. In section 5, the net radiative flux at the top of the atmosphere was specified from GCM results. This quantity is more or less zonally symmetric and can be approximated by a cosine dependence on latitude, so that it is maximum at the equator, positive in the tropics, negative in higher latitudes and has zero integral over the domain of the atmosphere. In reality the net radiative flux responds to atmospheric temperature. Since this cannot be properly represented in a two-level model, and since the effect of such changes on the atmospheric model stress field would be insignificant, the choice of fixing this quantity best serves the purposes of simplicity and hypothesis testing for initial experiments.

From a given configuration of SST and ocean surface heat flux, the atmospheric model determines a midtropospheric vertical velocity field and, from this, a surface stress. Since only anomalies are used for coupling, a reference climatology velocity is subtracted. The model climatology of vertical velocity, calculated using averages of SST and surface flux over the last six months of the ocean climatology run, is shown in Fig. 9 for Climatology I. The regions of strongest rising motion correspond surprisingly well to the Western Pacific (Indonesian) Convergence Zone, the South Pacific Convergence Zone, the ITCZ, and even the "Central American" Convergence Zone. Over the eastern Pacific, there is weak upward motion rather than weak downward motion but this does not severely affect ENSO convergence and stress anomalies. It is worth pointing out that the strongest convergence occurs over the ocean, despite the fact that the net flux of energy into the atmosphere is considerably weaker over the tropical oceans than over land. Over the equatorial ocean, the net surface flux is downward, into the ocean, and this reduces the net flux available to force the atmosphere relative to land surfaces. However, the low gross moist stability over the warm SSTs more than compensates for this effect.

The time integration of the coupled model proceeds by running the ocean model with fixed wind stress for a certain period and averaging the SST and surface flux over this time. These averaged quantities are then used by the atmosphere to calculate a new stress anomaly field which is used for the next period of ocean integration. A coupling timestep of half a month was used in all integrations. For simplicity, the length of all months was set to 30 days and a year to 360 days. Because there is little variance in SST at short time scales in this model, the interval of the coupling could be made shorter if desired. If instabilities of the equatorial currents were present then it would be necessary to take some care in choosing the averaging period.

7. Coupled model experiments

The coupled experiments described in this section represent an exploration of a small portion of the parameter space of the coupled system, within the limitations imposed by computer resources and by the complexity of the system. Many of the quantities which are relevant to the behavior of the coupled system, for instance the strength of the climatological upwelling, are not parameters which can be directly controlled but rather are internal variables which would change in a complex manner in response to parameters such as the vertical mixing coefficients of the ocean model. The "parameters" which have been varied in these initial runs have been chosen somewhat artificially, with the aim of mapping out some of the gross features of

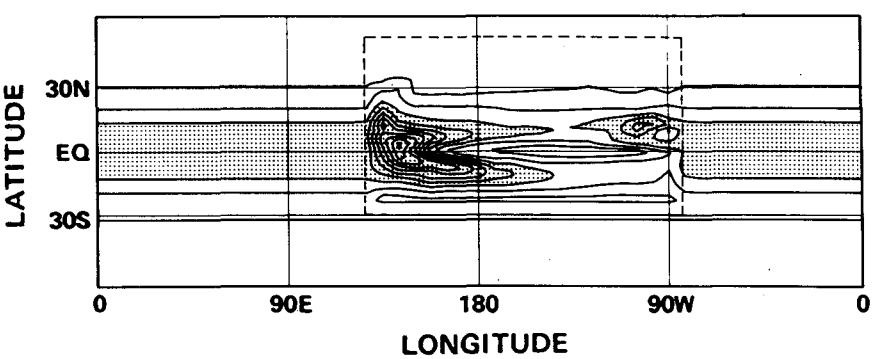

FIG. 9. The climatological vertical velocity from the atmospheric model, forced by mean SST and surface flux from ocean model Climatology I (contour interval 2×10^{-4} mb s^{-1}, shaded over 4×10^{-4} mb s^{-1}). The full domain of the atmospheric model is shown; global in longitude and up to 63° latitude. The boundary of the ocean basin is indicated by the dashed line. Idealized boundary conditions are specified outside of the ocean basin.

the behavior of the coupled system. For instance, the strength of both the climatological and anomalous wind stress are varied by use of arbitrary coefficients. These become crude, but understandable, parameters which summarize the gross differences that might be found in different versions of a model modified by much more complex changes in physical parameterizations.

Table 1 summarizes the experiments numbered Runs I through VII, to be presented. The three climatologies used are those described in section 3, with the atmospheric model climatology constructed from the ocean climatology in each case, as described in section 6. The most important comparisons are, first, between Runs I and II, and, second, the series Run-II through Run-V. In the Run-I vs Run-II comparison, the parameter which is varied is the strength of the climatological wind stress; the wind stress specified in Clim-II is reduced by a factor of 0.6 relative to that of Clim-I. The differences in the two climatologies prove to be very significant to the existence of interannual oscillations. In the series of Runs II–V, a convenient parameter is provided by intervening in the atmospheric model. The wind stress anomaly that results from a given oceanic state is simply multiplied by a constant factor. This factor then becomes a *relative coupling coefficient* of the system for a given oceanic climatology. Taking the value of this relative coupling coefficient to be 1.0 for the unmodified atmospheric model used in Run-II, the coupling is reduced in successive steps until, in Run-V, the anomalous winds are reduced by the same factor as the mean wind stress relative to Run-I. Effects on the stability of the system are thus shown in a controlled manner. Changes in this parameter are more computationally efficient than changes in climatology since there is no need to integrate a new climatology to equilibrium for each experiment.

The experiments are each begun from the end of one of the climatological runs. An initial westerly wind stress anomaly is applied for one month, just as for the ocean-only experiment in section 4 with the exception of Run-VI. In this case, the same spatial pattern of the initial wind stress anomaly is used but the magnitude is reduced from 0.3 dyn cm^{-2} to 0.01 dyn cm^{-2}, which for numerical purposes may be regarded as an infinitesimal perturbation. The coupled system continues to evolve freely after this stress is switched off in each case.

Run I was begun from Clim-I (the standard climatology) with the atmospheric model parameters as in section 5. The time evolution of the SST field is shown in Fig. 10 as a function of longitude along the equator over the nine years of the run. The behavior contrasts sharply with that of the ocean-only run of Fig. 4. Initially, the acceleration of currents and eastward expansion of warm SST occur in much the same manner as the ocean-only run and a very similar evolution of Kelvin and Rossby wave packets may be seen in the current fields (not shown). However, the SST perturbations in the ocean-only case die out within a few months, whereas in the coupled run the initial warm phase continues for almost ten months. When it decays, rather than equilibrate, it overshoots and the system goes into a cold phase in which the equatorial cold tongue extends further west than normal, cutting into the Indonesian warm pool. The subsequent warm phase and cold phase are weaker than the first and the perturbation dies out by the time of the third warm phase. The time scale of this evolution is a property of the coupled system rather than of the ocean alone and the behavior is quite clearly that of a damped oscillation with a period of about 40 months.

In Run-II, the ocean climatology of the system's stationary point has been replaced by Clim-II, in which the specified climatological wind stress has been reduced by a factor of 0.6 relative to Clim-I. This change was motivated partly by the hypothesis that the overly strong equatorial cold tongue found in Clim-I was impeding sustained coupled oscillations and the specified wind stress provides a simple and direct means of influencing this. Further motivation is provided by the fact that some AGCM wind stress climatologies are weaker than observed and by the suspicion that the relative strengths of climatological versus anomalous wind stress might be an important factor in the coupled system.

As may be seen in Fig. 11, the effects of this change are dramatic. The SST evolution along the equator over the fifteen years of this run displays sustained and very strong oscillations. Two main modes of variability are found. The first has a period of just under four years and resembles the damped oscillation found in Run I.

TABLE 1. Coupled Model Experiments. See text for explanation of *Relative coupling coefficient*. Climatologies are described in section 3.

Experiment	Run-I	Run-II	Run-III	Run-IV	Run-V	Run-VI	Run-VII
Climatology*	Clim-I	Clim-II	Clim-II	Clim-II	Clim-II	Clim-II	Clim-III
Relative coupling coefficient	1.0	1.0	0.8	0.7	0.6	0.8	1.0
Initial stress anomaly	standard	standard	standard	standard	standard	infinitesimal	standard
Figure	10	11	12	13	14	—	15

* Climatology-II: specified climatological wind stress reduced relative to Clim-I; Climatology-III: mean equatorial heat content increased relative to Clim-I.

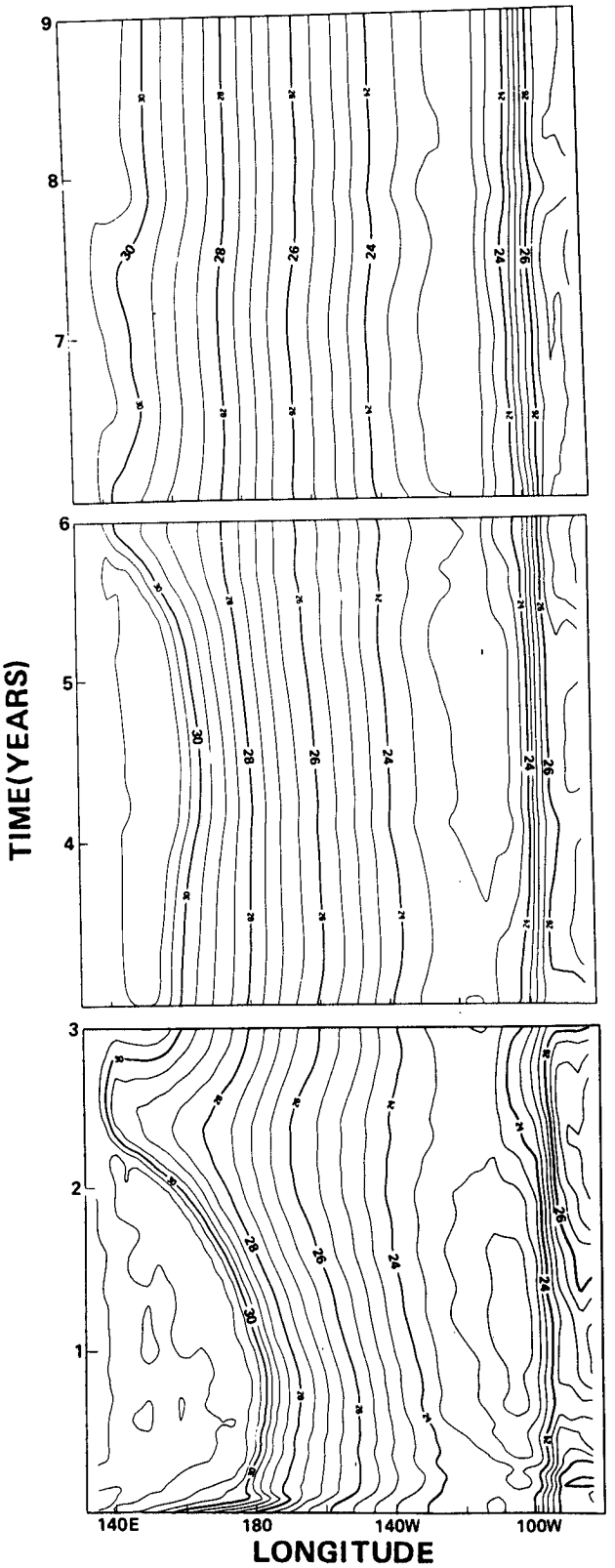

FIG. 10. Coupled model Run I: SST evolution along the equator. Time-longitude plots of the nine year integration. From Clim-I, relative coupling coefficient 1.0 (see text for explanation).

The second has a period of about five or six months and appears most strongly during the warm phase of the long period oscillation. The resemblance between the sustained El Niño-period oscillation in this run and the damped oscillation in the previous run suggests that the system has undergone a Hopf bifurcation leading from a stable stationary point with the 3 to 4 year oscillation weakly damped, to a state where the stationary point is unstable to this oscillation. If this is the case, it seemed reasonable to expect that for values of the parameters such that the stationary point is only weakly unstable, a less complex cycle will occur.

Run-III repeats Run-II, but with the relative coupling coefficient set to 0.8, where Run II has been defined to have a value of unity. The evolution of the SST during the nine years of this run, shown in Fig. 12, is very regular, with a period of just over three years. The evolution of the oscillation resembles that of the long period oscillation of Run-II, but has smaller amplitude and the six month oscillation has disappeared. The simpler structure and evolution of this oscillation at this parameter setting make it a reasonable target for experiments designed to elucidate the mechanism of the oscillation in future work.

Figures 13 and 14 show the behavior of the oscillation when the relative coupling coefficient is further reduced to 0.7 and 0.6 (Runs IV and V), respectively. The period remains virtually unchanged at close to three years, while the boundary between damped and sustained oscillations is crossed between these two values; at 0.7 the oscillation is sustained as a periodic limit cycle, while at 0.6 the oscillation decays to the stationary point which is stable. The resemblance in spatial form and period of the low-amplitude, sustained oscillation in Run-IV to the slowly decaying oscillation in Run-V provides good numerical evidence that the El Niño-period limit cycle arises as a Hopf bifurcation from the climatological stationary point; in other words, that the period of the oscillation is approximately that of the pair of eigenmodes of the system linearized about the climatological stationary point which are neutrally stable at the bifurcation. For values of the parameter slightly above the bifurcation, the stationary point is unstable and the unstable normal mode equilibrates into a limit cycle. Within some neighborhood above the bifurcation, the limit cycle inherits the period and structure of the eigenmodes at the bifurcation and these remain relatively constant as the amplitude of the limit cycle increases with increasing coupling. Similarly, slightly below the bifurcation, the most slowly decaying mode has approximately this same period and structure. At much higher coupling, as in Run-II, nonlinearity begins to affect the form and period of the limit cycle more strongly.

The linear normal mode stability analysis is impractical in a model of this size with a three-dimensionally varying basic state. To verify that the oscillations indeed arise from a linear instability of the sta-

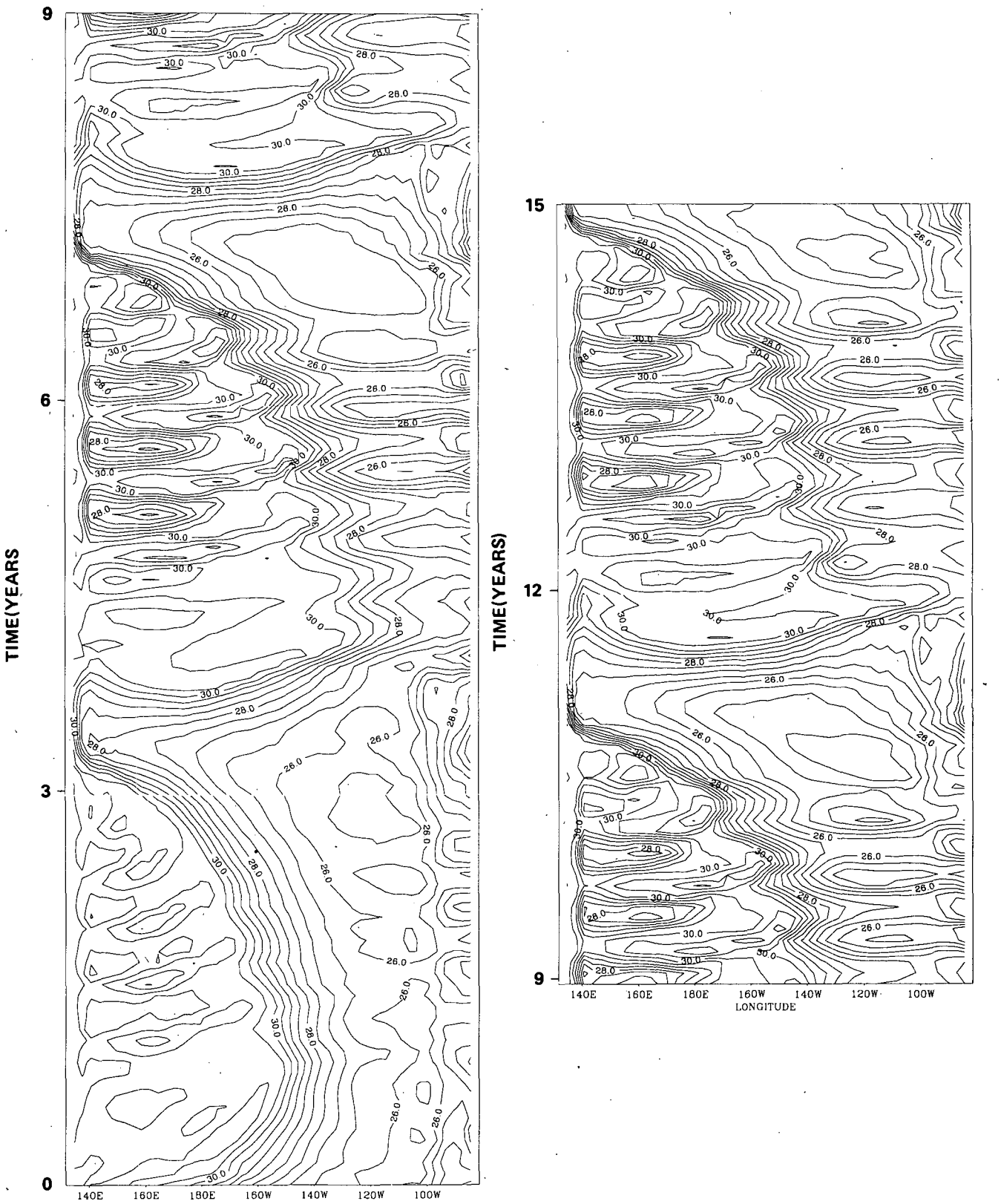

FIG. 11. As for Fig. 10 but for coupled Run II (15-year integration). From Clim-II, relative coupling coefficient 1.0.

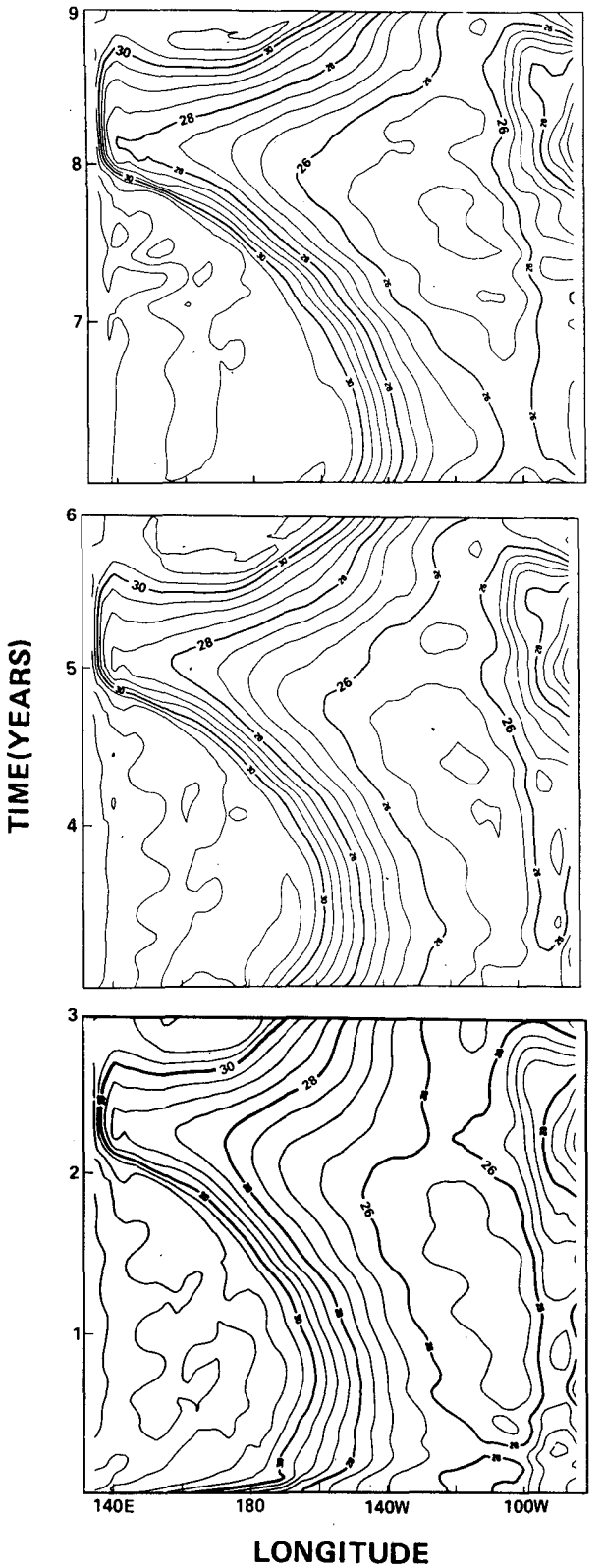

FIG. 12. As for Fig. 10 but for coupled Run III (9-year integration). From Clim-II, relative coupling coefficient 0. 8.

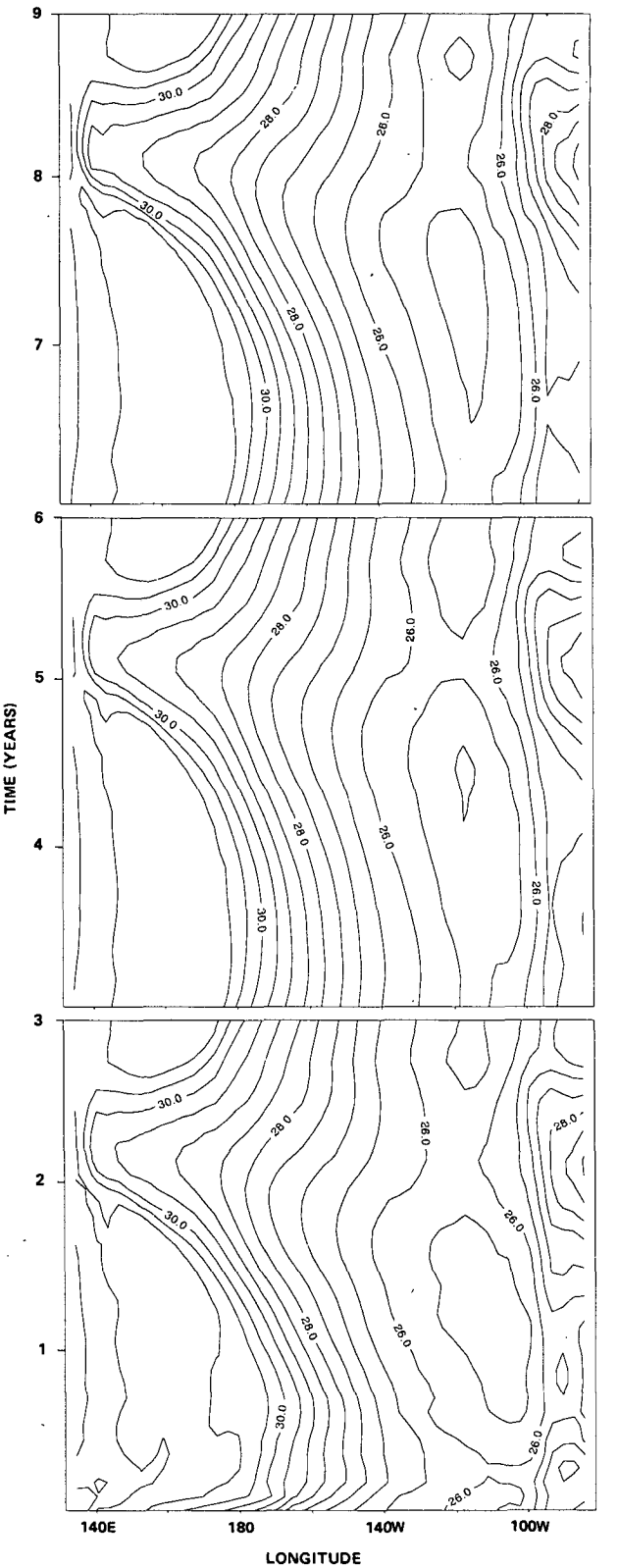

FIG. 13. As for Fig. 10 but for coupled Run IV (9-year integration). From Clim-II, relative coupling coefficient 0.7.

tionary point, Run-VI repeated the first three years of Run III but with the magnitude of the initial stress perturbation reduced to 0.01 dyn cm^{-2}, which may be regarded as an infinitesimal perturbation. The perturbation grew roughly exponentially, as expected, with an *e*-folding time of about three months.

Finally, one additional experiment (Run-VII) was conducted to see if increasing the heat content of the basic state (Clim-III) would favor coupled oscillations. The SST evolution over five years of the run in Fig. 15 shows a similar coupled evolution of the initial warm and cold phases but the subsequent warm phase never fully develops and the oscillation damps out even more quickly than in Run I. The changes in thermocline structure associated with the larger heat content in the basic state have acted to *increase* its stability, placing the system further below the bifurcation than Run I. A likely reason for this is the decrease in the vertical temperature gradient within the layer which can be

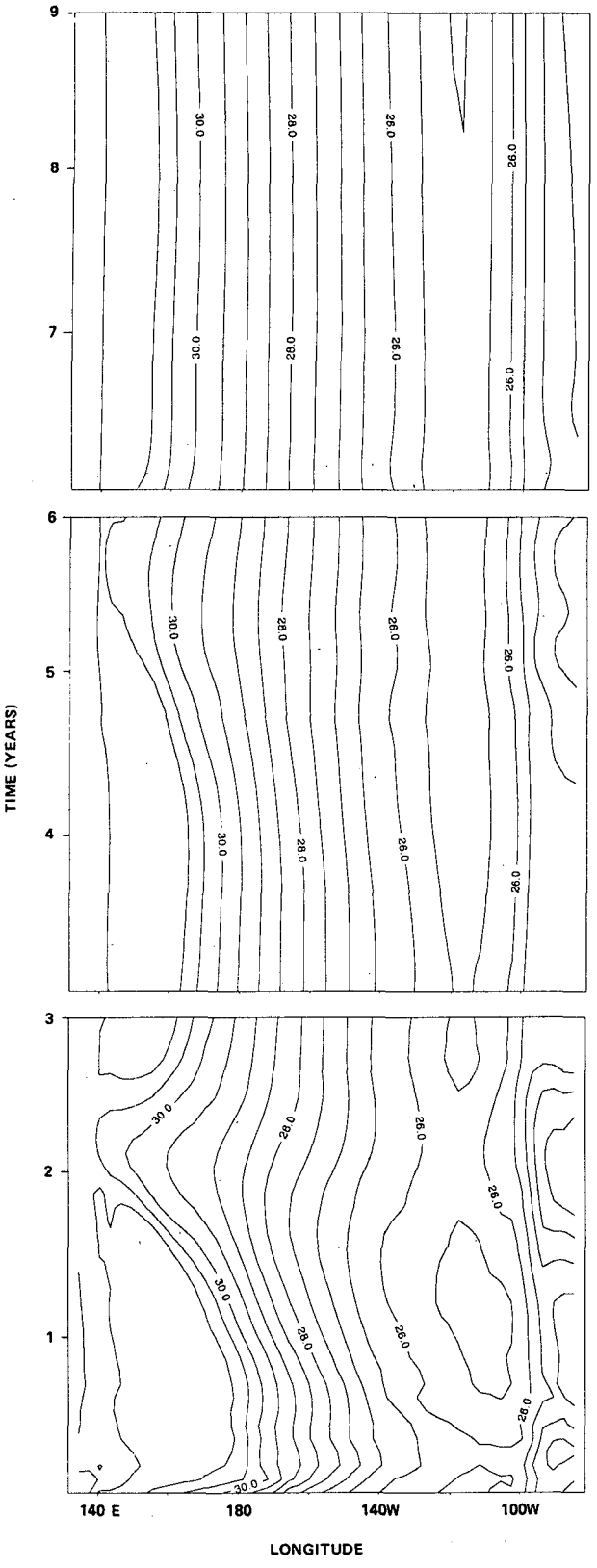

FIG. 14. As for Fig. 10 but for coupled Run V (9-year integration). From Clim-II, relative coupling coefficient 0.6.

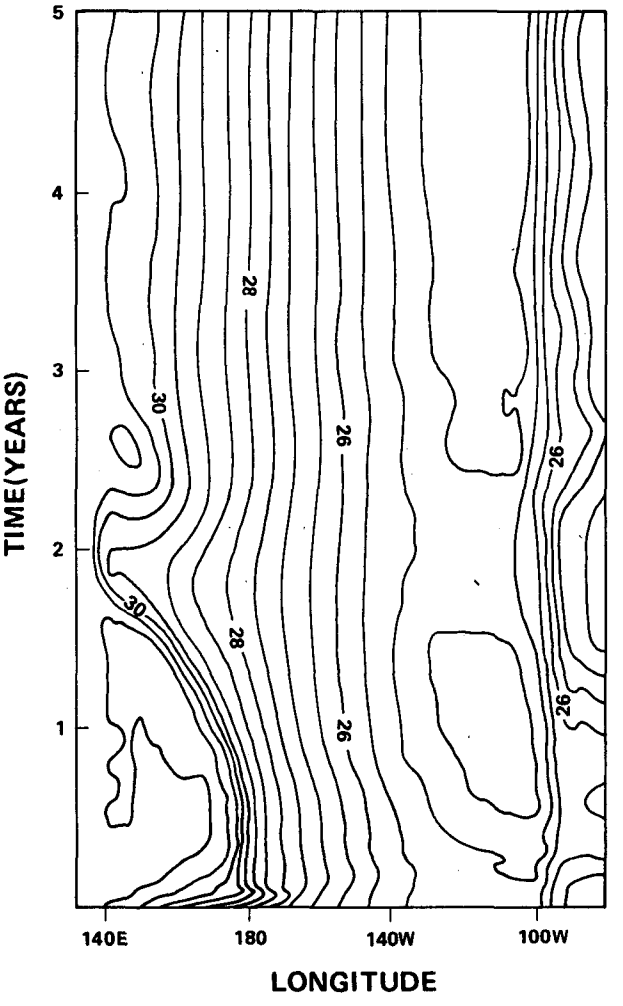

FIG. 15. As for Fig. 10 but for coupled Run-VII (5-year integration). From Clim-III, relative coupling coefficient 1.0.

accessed by equatorial upwelling (the upper 100–150 m).

8. Discussion

The numerical behavior of the coupled model as the relative coupling coefficient is varied may be used to infer a partial bifurcation diagram of the system as a function of this parameter. The stationary point corresponding to the climatology exists for all values, but above the first Hopf bifurcation, which occurs for a critical value of the relative coupling parameter between 0.6 and 0.7, it is unstable and the attractor of the system is the El Niño-period limit cycle corresponding to the equilibrated unstable coupled mode. As this parameter is increased, the limit cycle grows in amplitude and undergoes a secondary bifurcation, in which the singly periodic solution becomes unstable to a higher frequency coupled mode which appears most strongly during the warm phase of the El Niño oscillation. The secondary bifurcation is almost certainly also a Hopf bifurcation as evidenced by decaying oscillations of similar period in the initial warm phase of other runs.

The results of the series of experiments, Runs II–V, may thus be conveniently summarized on the schematic bifurcation diagram of Fig. 16. The ordinate is the amplitude of a suitably chosen variable characterizing the attractor as it cuts a plane in the model phase space (for instance, the projection of the model state onto one of the neutral modes at the Hopf bifurcation). The abscissa is the relative coupling coefficient. Below the Hopf bifurcation (labeled H), the constructed climatological stationary point of the system is stable (solid line). Above the bifurcation, it is unstable (dashed line) and the attractor is the El Niño-period limit cycle, shown as a parabolic curve as for a Hopf bifurcation in normal form. Between the values 0.8 and 1.0 of the relative coupling coefficient, this limit cycle itself goes unstable (dashed curve) to the five to six month oscillation at the secondary Hopf bifurcation (marked SH), above which the flow moves on a doubly periodic torus in the model phase space.

Such successive bifurcations are found in certain scenarios for the transition to chaos, but it is not clear whether this would occur within a realistic parameter range in this system. The oscillations found above the secondary bifurcation (Run II) appear complicated but are merely doubly periodic. Indeed, it appears that, rather than being quasi-periodic with two incommensurate frequencies, the oscillation in Run II is frequency-locked so that the six month oscillation repeats exactly the same pattern during every warm "El Niño" phase, once the oscillation settles down onto the attractor. Although the higher frequency oscillation in Run-II is much stronger than any corresponding variability in observations, there exists the possibility that such modes could exist but be marginally stable. Even if not actually unstable, such higher frequency modes could pose problems for prediction of El Niño in a system where initialization with sparse data and atmospheric noise have to be taken into consideration. One might note that oscillations of the central Pacific SST at six month intervals during the El Niño of 1986–87 had considerable negative impact on experimental predictions during that period (Barnett et al. 1988).

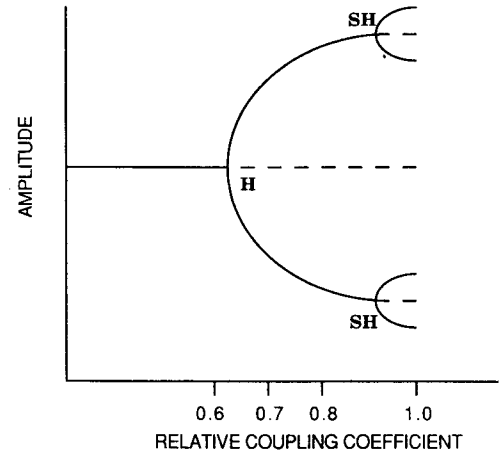

FIG. 16. Schematic bifurcation diagram for the coupled system, summarizing the results of Runs II through V (see text for explanation).

The similarity in period and spatial form of the oscillations in Runs III–V to the decaying oscillation in Run-I, together with the knowledge that the phase space flow is continuous in parameter space, strongly suggests that a bifurcation tree similar to Fig. 16 would also apply if the basic state were varied by small increments between the values of Run-I and Run-II. In this region of parameter space, the nature of the bifurcation implies that the stability or degree of instability of the climatology is sensitive to the basic state and coupling parameters but the period of the resulting oscillations is much less so.

The strength of the climatological wind stress affects the climatological stationary point of the coupled system in several ways: the strength of the equatorial upwelling is reduced; the surface temperature in the cold tongue region is increased; and the strength of the equatorial currents is slightly reduced. Because the balances maintaining the climatological zonal currents are quite nonlinear, the changes in these currents associated with the reduction in wind stress are small (order of 10% compared to a 40% reduction in stress and upwelling) and it is likely that the effect of these changes on the coupled instability is negligible. A coupled instability mechanism involving the $u'\bar{T}_x$ term of a linearized SST equation, where prime denotes perturbations and overbar denotes climatology, was considered by Hirst (1986) in a shallow water model. This is certainly not the responsible mechanism for the bifurcation in this case, since the zonal gradient of the climatological SST is smaller above the bifurcation. An

important source of instability in the Battisti (1988) version of the Cane and Zebiak (1985) model comes from the T'_{sub} part of the following term of the SST equation of that model, presented here in linearized form:

$$\bar{w}T'_z = \bar{w}(T' - T'_{sub})/H \quad (1)$$

where T' is the perturbation in SST and T'_{sub} denotes perturbations in subsurface temperature at depth H which are parameterized on thermocline depth perturbations in that model. Because the vertical structure of the temperature field below 50 m is little changed between Runs I and II while the mean upwelling is reduced, it seems likely that the tendency toward instability due to this mechanism is actually decreased in Run-II. The T'_{sub} term is therefore unlikely to be responsible for the bifurcation. However, the first term of (1), $\bar{w}T'/H$, acts as a strong damping on SST perturbations along the equator and so a reduction in $\bar{w}$ would tend to favor instability due to other terms. One candidate involves the term $w'\bar{T}_z$, since $\bar{T}_z$ is greater in Run-II than in Run-I. The importance of this term is suggested by the fact that Run-VII is further below the bifurcation than Run-I; the increase in equatorial heat content in this case leads away from instability because of the reduction in vertical temperature gradients in the layer over which vertical advection by anomalous upwelling acts. It is worth emphasizing that an increase in heat content along the equator in the basic state does not favor coupled instabilities in this model, due to the fact that heat content and vertical temperature gradients of the basic state are not independent parameters. More detailed analysis of the mechanism giving rise to the bifurcation will be the subject of further investigation.

These experiments show that the hybrid coupled GCM can produce sustained interannual oscillations whose period corresponds to the dominant time scale of El Niño. They also resemble ENSO in being equatorially trapped with temperature anomalies exhibiting both eastward and westward propagation along the equator during different phases of the cycle. However, the oscillations found in these experiments are not in perfect agreement with observed aspects of El Niño. The model cold phase propagates farther west than in the Rasmusson and Carpenter (1982) composites (although it more resembles the behavior of the 1988 cold phase). The observed warm phase is stronger in the east than the warm-phase of Run III, although Run II is better in this respect. In fact, as the relative coupling coefficient is increased, there is a systematic progression of the position of the warm phase maximum toward the east, so that runs with strong coupling correspond better to observations in this respect than do runs with weak coupling. In general, the warm phase of the oscillation is more reminiscent of the 1982–83 El Niño than of the canonical Rasmusson and Carpenter composite El Niño. The differences between this model and observations in the eastern basin are perhaps not surprising when one considers that the geography in this region has been idealized to a flat wall.

More importantly, these experiments serve to indicate something of the range of dynamics of the coupled system that one can expect to encounter in coupled GCMs and possibly also in nature. The crossing of the bifurcation from a stable climatology to a limit cycle with sustained El Niño oscillations may be extremely relevant to the results of a recent CGCM experiment at MPIM by Latif et al. (1988). In this experiment, a westerly wind stress anomaly is imposed in the western Pacific during the first month of the run, very much as in the experiments described above. The warm phase initiated by this wind burst is maintained over much of the subsequent year of the coupled run—much longer than occurs in an ocean-only control experiment—but eventually decays. No sustained El Niño cycle is found in this model over the course of a ten year run (Latif et al. 1988). It may be hypothesized that the MPIM model is in the regime of Runs I, V, and VII in which the ENSO mode of oscillation decays with time rather than leading to a limit cycle through instability of the climatology. A striking feature of the ocean climatology in the MPIM model is a very strong equatorial cold tongue in which the SST is 4°C colder than observations. In the HGCM, the reduction in strength of the climatological cold tongue of Run-I apparently leads to the sustained oscillations of Run-II. This is rather suggestive with regard to the MPIM coupled model. If the problem of the cold tongue in the ocean climatology could be corrected, it seems very possible that a similar bifurcation would occur, leading to sustained coupled oscillations.

On the other extreme, the CGCM of Philander et al. at GFDL (1989) appears to be in an even more strongly coupled regime than has been explored in the HGCM. It alternates between warm and cold phases with a characteristic time scale considerably longer than three years and has a great deal of variance associated with a higher frequency one year oscillation. While this variance could be the result of atmospheric noise, it is tempting to speculate that it could arise as a secondary bifurcation, much like the six month oscillation in the HGCM.

It is not clear which regime in parameter space best corresponds to observed interannual variability. In a system perturbed by atmospheric noise, a considerable, irregular interannual signal could occur even slightly below the first bifurcation, excited by atmospheric events. The three year period of the slowly decaying modes in the deterministic system would also characterize the noise-forced variability in the stochastically perturbed system. Above the bifurcation, noise would perturb the limit cycle to a greater or lesser extent depending on the characteristics of the noise and the time scale of decay toward the attractor. Because the decay time scales in the vicinity of the attractor in the deterministic system would apply also in the stochastically perturbed system, one can anticipate large sensitivity

to noise near the bifurcation, both below and above. It is also likely that the complex attractor found in the regime of Run III would be strongly affected by stochastic forcing of realistic variance. Producing the irregular behavior of the observed ENSO time series should be possible even with relatively modest amounts of noise, although this cannot be answered without quantitative investigation. In any case, the complexity of the behavior found in these experiments amply justifies investigation of the deterministic system, to better understand the stochastically perturbed counterpart encountered in the coupled GCMs.

Acknowledgments. This work was supported by NSF Grants ATM-8905164 and ATM-8342482 and by the Canadian National Science and Engineering Research Foundation. Part of this work was carried out during a postdoctoral year at the Department of Earth, Atmospheric and Planetary Sciences, Massachusetts Institute of Technology, during which the support and encouragement of Richard Lindzen are gratefully acknowledged. The author thanks George Philander for much discussion, access to ocean GCM code and computing time at the Geophysical Fluid Dynamics Laboratory where some of the model integrations were carried out. Work on the atmospheric model was also carried out at GFDL, and thanks are due to Isaac Held and Gabriel Lau for discussions important to this section. Ron Pacanowski provided advice on GCM code and Fabrice Cuq assisted with computer graphics. Conversations with Michael Ghil, Mark Cane and David Battisti are also appreciated. Acknowledgement is made to the National Center for Atmospheric Research, which is sponsored by the National Science Foundation, for computing time used in this research. This work, like many others, owes a debt to the memory of Michael Cox and his contribution to ocean model development.

REFERENCES

Anderson, D. L. T., and J. P. McCreary, 1985: Slowly propagating disturbances in a coupled ocean-atmosphere model. *J. Atmos. Sci.*, **42**, 615–629.

Barnett, T., N. Graham, M. Cane, S. Zebiak, S. Dolan, J. O'Brien and D. Legler, 1988: On the prediction of the El Niño of 1986–1987. *Science*, **241**, 192–196.

Battisti, D. S., 1988. The dynamics and thermodynamics of a warming event in a coupled tropical atmosphere/ocean model. *J. Atmos. Sci.*, **45**, 2889–2919.

Bryan, K., 1969: A numerical method for the study of the world ocean. *J. Comp. Phys.*, **4**, 347–376.

——, and M. D. Cox, 1968: A nonlinear model of an ocean driven by wind and differential heating: Part I. *J. Atmos. Sci.*, **25**, 945–967.

Cane, M. A., and S. E. Zebiak, 1985: A theory for El Niño and the Southern Oscillation. *Science*, **228**, 1084–1087.

Davey, M. K., and A. E. Gill, 1987: Experiments on tropical circulation with a simple moist model. *Quart. J. Roy. Meteor. Soc.*, **113**, 1237–1269.

Gill, A. E., 1980: Some simple solutions for heat induced tropical circulation. *Quart. J. Roy. Meteor. Soc.*, **106**, 447–462.

Harrison, E., 1989: On climatological monthly mean wind stress and wind stress curl fields over the world ocean. *J. Climate*, **2**, 57–70.

Hellerman, S., and M. Rosenstein, 1983: Normal monthly windstress over the world ocean with error estimates. *J. Phys. Oceanogr.*, **13**, 1093–1104.

Hirst, A. C., 1986: Unstable and damped equatorial modes in simple coupled ocean-atmosphere models. *J. Atmos. Sci.*, **43**, 606–630.

Latif, M., J. Biercamp and H. von Storch, 1988: The response of a coupled ocean-atmosphere model to wind bursts. *J. Atmos. Sci.*, **45**, 964–979.

Lau, N.-C., 1985: Modelling the seasonal dependence of the atmospheric response to observed El Niños in 1962–76. *Mon. Wea. Rev.*, **113**, 1970–1996.

Levitus, S., 1982: *Climatological Atlas of the World Ocean.* NOAA professional paper no. 13, 173 pp., 17 microfiche, U.S. Government Printing Office, Washington, D.C.

Lindzen, R. S., and S. Nigam, 1987: On the role of sea surface temperature gradients in forcing low level winds and convergence in the tropics. *J. Atmos. Sci.*, **45**, 2440–2458.

Manabe, S., D. G. Hahn and J. L. Holloway, 1974: The seasonal variation of the tropical circulation as simulated by a global model of the atmosphere. *J. Atmos. Sci.*, **31**, 43–83.

Matsuno, T., 1966: Quasi-geostrophic motions in the equatorial area. *J. Meteor. Soc. Japan, Ser. II*, **44**, 25–43.

Neelin, J. D., 1988: A simple model for surface stress and low level flow in the tropical atmosphere driven by prescribed heating. *Quart. J. Roy. Meteor. Soc.*, **114**, 747–770.

——, 1989: On the interpretation of the Gill model. *J. Atmos. Sci.*, **46**, 2466–2468.

——, and I. M. Held, 1987: Modelling tropical convergence based on the moist static energy budget. *Mon. Wea. Rev.*, **115**, 3–12.

Philander, S. G. H., 1976: Instabilities of zonal equatorial currents. *J. Geophys. Res.*, **81**, 3725–3735.

——, 1978: Instabilities of zonal equatorial currents, 2. *J. Geophys. Res.*, **83**, 3679–3682.

——, 1981: The response of the equatorial oceans to a relaxation of the trade winds. *J. Phys. Oceanogr.*, **11**, 176–189.

——, N. C. Lau, R. C. Panowski and M. J. Nath, 1989: Two different simulations of the Southern Oscillation and El Niño with coupled ocean–atmosphere general circulation models. *Phil. Trans. Roy. Soc. London*, **A329**, 167–178.

——, and R. C. Pacanowski, 1980: The generation of equatorial currents. *J. Geophys. Res.*, **85**, 1123–1136.

——, and ——, 1981a: Parameterization of vertical mixing in numerical models of the tropical oceans. *J. Phys. Oceanogr.*, **11**, 1443–1451.

——, and ——, 1981b: Response of the equatorial ocean to periodic forcing. *J. Geophys. Res.*, **86**, 1903–1916.

——, and ——, 1984: Simulation of the seasonal cycle in the tropical Atlantic ocean. *Geophys. Res. Lett.*, **II**, 802–804.

——, and A. D. Siegel, 1985: Simulation of El Niño of 1982–1983. *Coupled Ocean-Atmosphere Models, Elsevier Oceanography Series, 40*, J. C. J. Nihoul, Ed., Elsevier.

——, T. Yamagata and R. C. Pacanowski, 1984: Unstable air–sea interactions in the tropics. *J. Atmos. Sci.*, **41**, 604–613.

——, W. J. Hurlin and A. D. Siegel, 1987: Simulation of the seasonal cycle of the tropical Pacific ocean. *J. Phys. Oceanogr.*, **17**, 1986–2002.

Rasmusson, E. M., and T. H. Carpenter, 1982: Variations in tropical sea surface temperature and surface wind fields associated with the Southern Oscillation/El Niño. *Mon. Wea. Rev.*, **110**, 354–384.

Schopf, P. S., and M. J. Suarez, 1988: Vacillations in a coupled ocean–atmosphere model. *J. Atmos. Sci.*, **45**, 549–566.

Webster, P. J., 1981: Mechanisms determining the atmospheric response to sea surface temperature anomalies. *J. Atmos. Sci.*, **38**, 554–571.

Zebiak, S. E., 1986: Atmospheric convergence feedback in a simple model for El Niño. *Mon. Wea. Rev.*, **114**, 1263–1271.

——, and M. A. Cane, 1987: A model ENSO. *Mon. Wea. Rev.*, **115**, 2262–2278.